文章编号:1000-8055(2014)02-0467-08 doi:10.13224/j.cnki.jasp.2014.02.028

Numerical simulation of viscous flows with adaptively refined Cartesian grid

HAN Yu-qi, GAO Ge

(National Key Laboratory of Science and Technology on Aero-Engine Aero-thermodynamics,
School of Energy and Power Engineering,
Beijing University of Aeronautics and Astronautics, Beijing 100191, China)

Abstract: Quadtree-based Cartesian grid was automatically generated from specified geometry. Adaptive refinements were performed according to geometric parameters and solution of flow field. An altered CCST (curvature corrected symmetry technique) approach was proposed to apply solid wall boundary conditions. Driven flows in a square cavity and flows around NACA0012 airfoil were simulated and compared with the result of published structured grid and stretched Cartesian grid. The results show that solid wall boundary condition are accurately applied by current altered CCST approach, while incompressible/compressible subsonic, transonic and supersonic viscous flows are adequately simulated with adaptively refined Cartesian grid.

Key words: adaptively refined; Cartesian grid; viscous flow;
CCST (curvature corrected symmetry technique); boundary condition

CLC number: V211.3 **Document code**: A

Grid generation is a great challenge for complicated geometric configurations in CFD. Body-fitted structured grid is concise in data structure and convenient in implementing boundary conditions while laborious artificial labors are inevitable for complex regions. Body-fitted unstructured grid can rapidly establish the grid while suffering with inefficient data storage and solving. Compared with body-fitted grid, Cartesian grid has prominently less operations per cell, lower storage space and easier in dealing with arbitrary boundaries, which enormously aroused the interest of scholars. As Cartesian grid can extend through the geometric surface which produces irregular cut cells, accurate imposition of the solid wall boundary condition is essential for its success in CFD.

Zeeuw, Coirier and Colella, et al[1-3] used embedded boundary method to represent solid wall, irregular cut cells were determined by the polygon clipping algorithm. Udaykumar, Hua, et al[4-5] used merged cell approach which combined the small cut cell and its neighbor cell to be a larger one. Both of them ensured the conservation of cut cell but complicated the data structure and solving. Kirshman, Luo and Liao, et al[6-8] employed least-squares fitting to calculate the numerical flux of boundary cells which was termed gridless method, other flow cells were solved with Cartesian grid. This approach effectively reduced the difficulty of the boundary treatment, but the boundary cells were computational expensive and conservation cannot be guaranteed. Dadone and Grossman proposed the CCST approach on structured grid to treat the solid wall, which was further extended to Cartesian grid and termed with GBCM (ghost body-cell method)[9-10]. This approach employed reflect point to impose boundary conditions and had minimal computational cost as the cut cells and other flow field cells were treated in the same way, but the conservation of boundary

Received: 2012-12-21

E-mail: hanyuqi@sjp.buaa.edu.cn

cells couldn't be ensured either. Relative entropy error was dramatically reduced and second order of accuracy was achieved with CCST method.

Current research aims to extend the CCST approach to adaptively refined Cartesian grid in the simulation of viscous flows. Quadtree-based data structure is converted to linear data structure according to the Morton space filling theory[11] for efficiency. AMR (adaptively mesh refinement) are automatically performed based on geometrical information and solution of flow field. Flows in the driven cavity and around the NACA0012 airfoil are simulated and compared with published results, which validate its capability in the simulations of incompressible/compressible viscous flows.

1 Adaptively refined Cartesian grid generation

Concrete steps are as follows:

1) The computational domain is uniformly divided to generate coarse base grid.

2) Cut cell adaption. Cut cells are produced by the intersection of grid and geometric interfaces. These cells and their nearest two layers of neighbor cells are refined to increase the resolution of solid wall.

3) Curvature cell adaption. Cells near the geometric point with big radius of curvature are to be refined. The criterion employed here is $\max(\Delta x,\Delta y) < (1/40)R$, where R is the radius of curvature, Δx and Δy are local lateral and longitudinal length scales, respectively.

4) Solution adaption. The criterion proposed by Zeeuw[1] is employed:

$$\tau_{ci} = |\nabla \times \mathrm{U}| l_i^{\frac{r+1}{r}}, \quad \tau_{\mathrm{d}i} = |\nabla \cdot \mathrm{U}| l_i^{\frac{r+1}{r}} \tag{1}$$

$$\sigma_{\mathrm{c}} = \sqrt{\frac{\sum_{i=1}^{n} \tau_{ci}^2}{n}}, \quad \sigma_{\mathrm{d}} = \sqrt{\frac{\sum_{i=1}^{n} \tau_{\mathrm{d}i}^2}{n}} \tag{2}$$

Where empirical coefficient r is taken to be 1.5 here, l_i is the local cell's length scale, and U is the velocity of flow. If either $\tau_{ci} > \sigma_{\mathrm{c}}$ or $\tau_{\mathrm{d}i} > \sigma_{\mathrm{d}}$, the cell i will be refined.

2 Numerical methods

2.1 Governing equations

Two-dimensional unsteady dimensionless N-S (Navier-Stokes) equations can be written as:

$$\frac{\partial u_m}{\partial t} + \frac{\partial (f_m - f_{vm})}{\partial x} + \frac{\partial (g_m - g_{vm})}{\partial y} = 0 \tag{3}$$

Where

$$[u_1, u_2, u_3, u_4] = [\rho, \rho u, \rho v, \rho e],$$

$$[f_1, f_2, f_3, f_4] = [\rho u, \rho u^2 + p, \rho uv, (\rho e + p)u],$$

$$[g_1, g_2, g_3, g_4] = [\rho v, \rho vu, \rho v^2 + p, (\rho e + p)v],$$

$$[f_{v1}, f_{v2}, f_{v3}, f_{v4}] = [0, \tau_{xx}, \tau_{xy}, u\tau_{xx} + v\tau_{xy} - q_x],$$

$$[g_{v1}, g_{v2}, g_{v3}, g_{v4}] = [0, \tau_{xy}, \tau_{yy}, u\tau_{xy} + v\tau_{yy} - q_y],$$

$$\tau_{xx} = \frac{2}{3}\frac{Ma_\infty}{Re_\infty}\mu\left(2\frac{\partial u}{\partial x} - \frac{\partial v}{\partial y}\right),$$

$$\tau_{yy} = \frac{2}{3}\frac{Ma_\infty}{Re_\infty}\mu\left(2\frac{\partial v}{\partial y} - \frac{\partial u}{\partial x}\right),$$

$$\tau_{xy} = \frac{Ma_\infty}{Re_\infty}\mu\left(\frac{\partial u}{\partial y} + \frac{\partial v}{\partial x}\right),$$

$$q_x = -\left[\frac{Ma_\infty \mu}{Re_\infty Pr(\gamma - 1)}\right]\left(\frac{\partial T}{\partial x}\right),$$

$$q_y = -\left[\frac{Ma_\infty \mu}{Re_\infty Pr(\gamma - 1)}\right]\left(\frac{\partial T}{\partial y}\right)$$

Ma_∞ and Re_∞ are free stream Mach number and free stream Reynolds number, Pr is Prandtl number, γ is specific heat ratio, $\mu = T^n$ is the coefficient of viscosity; for the air, $n = 0.76$, $Pr = 0.72$, $\gamma = 1.4$. p, ρ, e, T are pressure, density, energy and temperature, u, v are velocity component along x- and y-direction, respectively. The dimensionless characteristic variables are density ρ_∞, temperature T_∞ and acoustic speed a_∞ of the free stream, the dimensionless length scale c is side length for driven cavity and chord length for airfoil, respectively. For perfect gas

$$p = \frac{\rho T}{\gamma} \tag{4}$$

Specific energy is

$$e = \frac{p}{\rho(\gamma - 1)} + \frac{u^2 + v^2}{2} \tag{5}$$

2.2 Numerical schemes

MUSCL (monotone upstream-centered schemes

for conservation laws) interpolation scheme and Van Leer limiter are employed to achieve second order of accuracy with finite volume method. Invisid flux is calculated by Liou's AUSM$^+$-up (advection upstream splitting method-up) scheme[12]. Viscous flux is calculated by Coirier's diamond-path reconstruction scheme[2].

Temporal terms are calculated by the three-stage Runge-Kutta scheme:

$$\begin{cases} U^{(0)} = U^n \\ U^{(k)} = U^{(0)} + \dfrac{\alpha_k \Delta t}{A} \mathrm{Res}(U^{(k-1)}) \\ k = 1,2,3 \\ U^{n+1} = U^{(3)} \end{cases} \tag{6}$$

Where $\alpha_1 = 0.18$, $\alpha_2 = 0.5$, $\alpha_3 = 1.0$.

2.3 Boundary conditions

Dadone and Grossman proposed the CCST method on structured grid to treat the solid wall, which is further extended to Cartesian grid and termed with GBCM[9-10]. Wang and Sun[13] applied it to simulate invisid flows on unstructured grid. Published numerical results by the previous scholars show that the CCST method is second order of accuracy and dramatically reduced the relative entropy error.

In Dadone's CCST method, centroid of the cell is used to classify its type, solid cell if it locates in solid domain and flow cell if it locates in flow domain. Flow variables at solid cells are calculated resort to their reflect point with respect to the solid boundary which locate in flow domain. The viscous flux of the cut flow cell is highly inaccurate as the cut cell extends through the solid surface, which leads to the failure of application with viscous CCST method on adaptively refined Cartesian grid. Here the flow variables at cut flow cell are not solved but interpolated to remedy this problem.

As in figure 1, point C is centroid of cut flow cell. A reference point R is specified which is in the normal direction of solid wall. The distance between point R and point C is $L = \sqrt{A}$, where A is area of the cut flow cell. The wall temperature condition uses enforced wall temperature $T_w = T_\infty^*$, where T_∞^* is the stagnation temperature of the free stream. No slip condition indicates that the velocity is zero at the solid wall. A linear distribution of velocity and temperature is assumed near the solid wall, integrate the normal momentum equation (7) and then we have relation equation (8):

$$\frac{\partial p}{\partial n} = \rho \frac{\tilde{u}^2}{R_c} \tag{7}$$

$$\begin{cases} p_C = p_R - \dfrac{(1-r^3)}{3}\left(\dfrac{\rho_R \tilde{u}_R^2}{R_c}\right) d_R \\ T_C = T_w + r(T_R - T_w) \\ \tilde{u}_C = r\tilde{u}_R \\ \tilde{v}_C = r\tilde{v}_R \end{cases} \tag{8}$$

Where R_c is the local radius of curvature. d_R, d_C are the distance of point R and point C to the solid wall, respectively. The distance ratio r is $r = d_C/d_R$. $p, \rho, T, \tilde{u}, \tilde{v}$ are pressure, density, temperature, tangential velocity and normal velocity, respectively. Flow variables at point R can be linearly interpolated using the variables of the nearest three flow cells. Then flow variables at point C can be decided through equation (8).

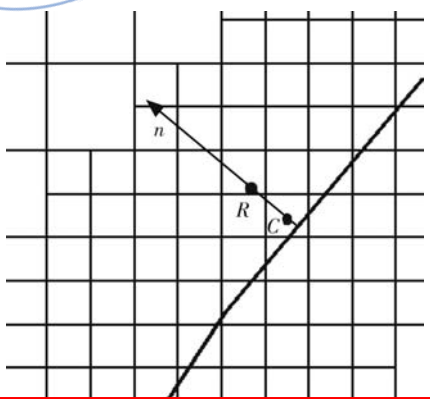

Fig. 1　Sketch of point C and point R

Flow variables of solid cells are obtained in a similar way. If point C denotes centroid of solid cell and point R denotes the reflect point of point C with respect to the solid wall, set $r = -1$ and then equation (8) can be used to decide the flow variables of solid cells.

Non-reflective boundary conditions based on characteristic analysis of one-dimensional Riemann invariants are employed to implement far-field boundary.

3 Numerical results and discussions

3.1 Square cavity

This case is a benchmark for incompressible viscous flow and has been carefully investigated by Ghia, et al[14] on a 129×129(16 641) uniform structured grid. The top lid moves horizontally right at speed $Ma=0.1$, which induces primary vortex in the central region and smaller vortices in the corner regions.

The results obtained with current approach for $Re=3\,200$ case are shown from figure 2 to figure 4, where c is the side length of the square cavity and U_{lid} is speed of the top lid. Figure 2 shows the initial computational grid for the square cavity. Figure 3 shows the grid after three solution adaptions, where can be seen that the cells in the strong shear regions have been well refined. The vortices are clearly shown by streamlines contours depicted by figure 4. Figure 5 and figure 6 show the u- and v-velocity profiles obtained along vertical and horizontal lines through the geometric center of the driven cavity (the number of cells at each refinement level is labeled in parenthesis). As can be seen, resolution of flow field has been improved by adaptive refinement technique and the results obtained on final grid agree well with Ghia's data. Finally, location of primary vortex center with different Reynolds number is shown in figure 7.

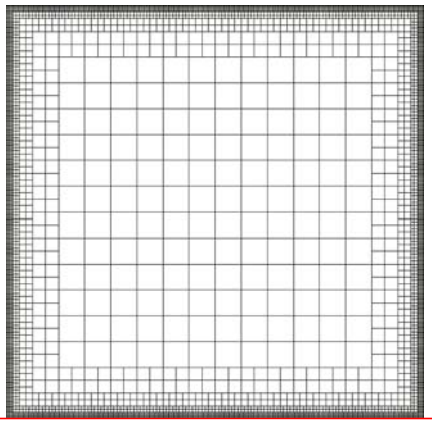

Fig. 2 Initial computational grid of the square cavity

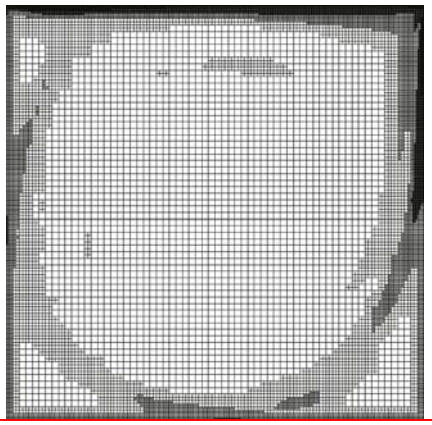

Fig. 3 Refinement level 3 adapted grid of the square cavity

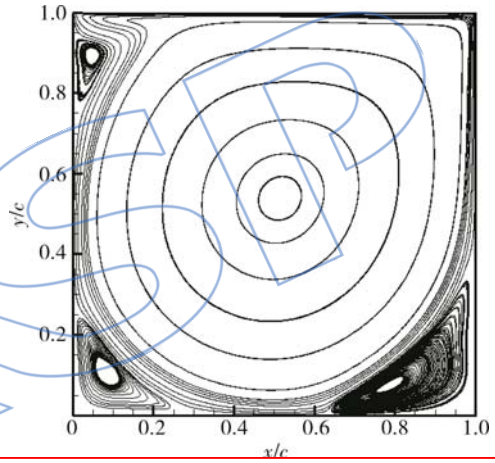

Fig. 4 Streamlines contours for the cavity flow

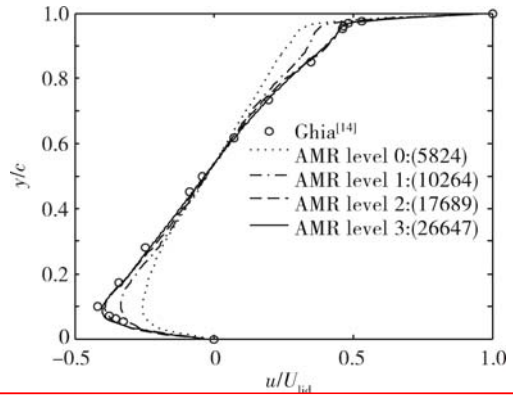

Fig. 5 u-velocity along vertical line through geometric center

3.2 NACA0012 airfoil

Flows around NACA0012 airfoil are simulated to validate the capability of current approach in transonic/supersonic compressible flows. The computational domain is $[-127.5c, -128c]\times$

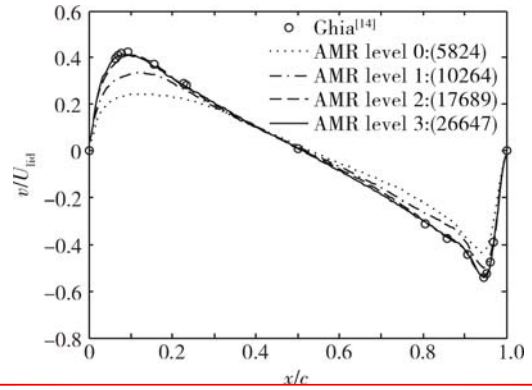

Fig. 6　v-velocity along horizontal line through geometric center

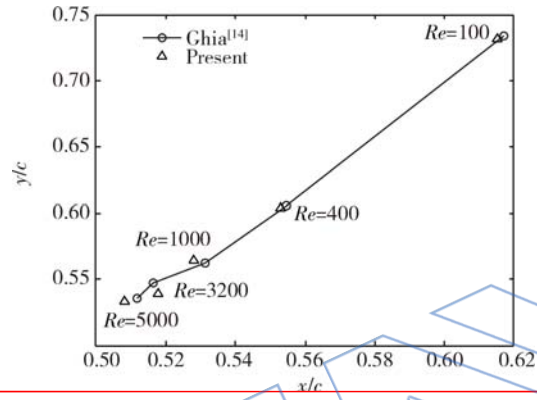

Fig. 7　Location of primary vortex center with different Re

$[128.5c, 128c]$ in the current research, where c is the chord length. In case 1, the free stream Mach number is 0.8, free stream Reynolds number is 500 and attack angle is 10°. In case 2, the free stream Mach number is 2.0, free stream Reynolds number is 1 000 and attack angle is 10°.

Case 1 has been simulated by Dadone[10] on a C-type structured grid with 256×64 (16 384) cells, and by LIU[15] on a stretched Cartesian grid with 287×298 (85 526) cells. The grid after four solution adaptions is shown in figure 8 which contains 32 582 cells. Mach number contours are shown in figure 9 which indicate that there is a large recirculation region on the upper surface of the NACA0012 airfoil. Figure 10 shows the pressure coefficient distributions on the surface of the NACA0012 airfoil, which agree well with published results. Figure 11 shows the skin friction coefficient distributions on the surface of the NACA0012 airfoil, only Dadone's results have been compared as LIU has not given the corresponding data. Streamlines in the separation region are shown in figure 12. Location of separation point is compared with

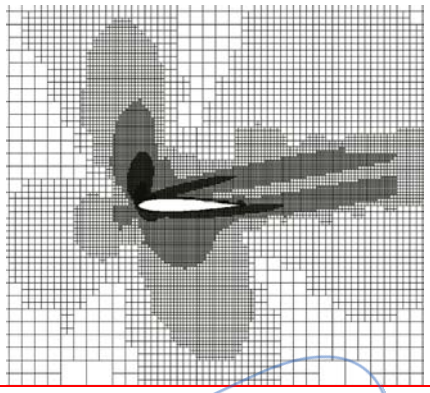

Fig. 8　Refinement level 4 adapted gird of the NACA0012 airfoil for case 1

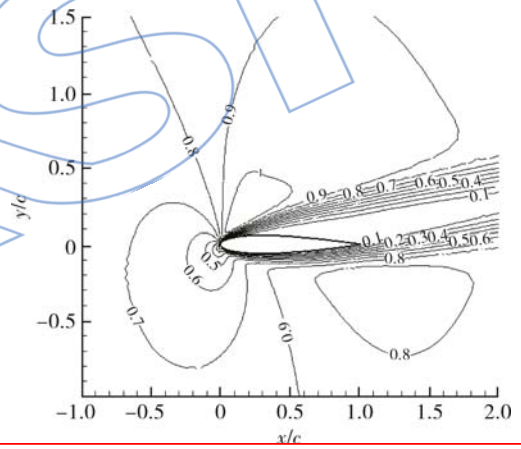

Fig. 9　Mach number contours of flow around the NACA0012 airfoil for case 1

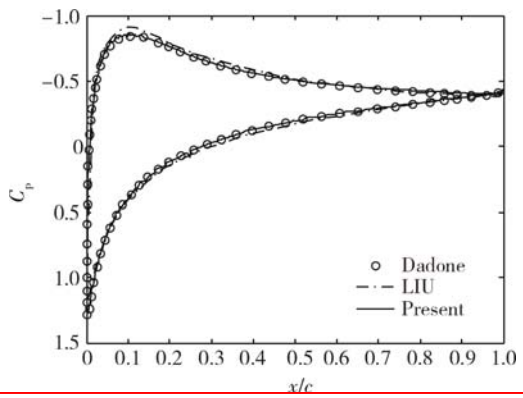

Fig. 10　Pressure coefficient distributions on the surface of the NACA0012 airfoil for case 1

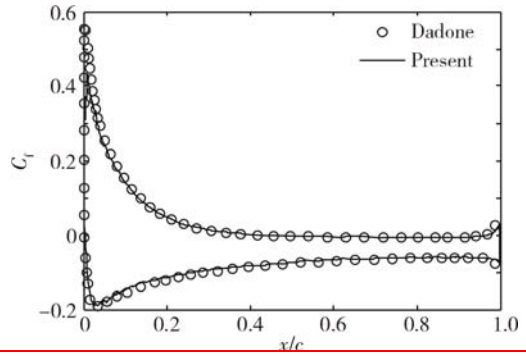

Fig. 11 Skin friction coefficient distributions on the surface of the NACA0012 airfoil for case 1

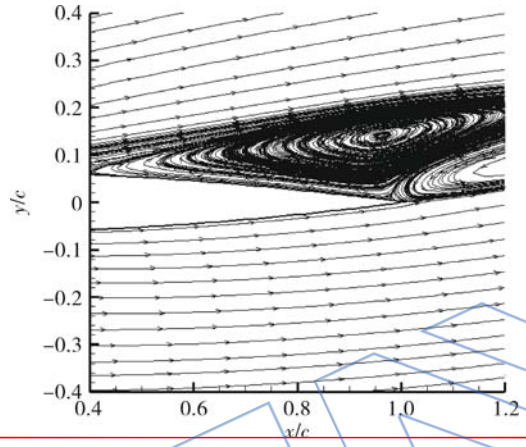

Fig. 12 Streamlines in the separation region of the NACA0012 airfoil for case 1

well-assessed results[16] and shown in table 1. Deviation appears at the leading edge of NACA0012 airfoil while good agreement was shown in an overall view.

Table 1 Abscissa of separation point

Author	Separation point
Angrand	0.5
Bristeau, et al	0.45
Cambier	0.36
Haase	0.36
Kalfon, et al	0.39
Kordulla	0.362
Muller, et al	0.371
Satofuka, et al	0.345
Secretan, et al	0.37
Present	0.389

Case 2 has been simulated by Palma, et al[17] on a stretched Cartesian grid with 500 × 500 (250 000) cells, and by LIU[15] on a stretched Cartesian grid with 287×298(85 526) cells. The grid after four solution adaptions is shown in figure 13 which contains 29 860 cells and Mach number contours are shown in figure 14 where a bow shock can be seen in front of the NACA0012 airfoil and the corresponding region has been well refined. Figure 15 shows the pressure coefficient distributions on the surface of the NACA0012 airfoil, which agree well with Palma's results. It is notable that current approach uses much less cells due to the adaptive refinement technique. Figure 16 shows the skin friction coefficient distributions on the surface of the NACA0012 airfoil by the current approach, while Palma and LIU has not given the corresponding data.

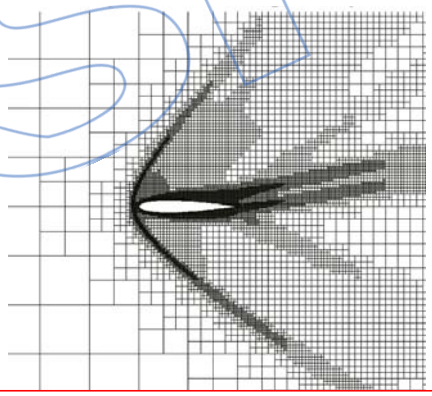

Fig. 13 Refinement level 4 adapted grid of the NACA0012 airfoil for case 2

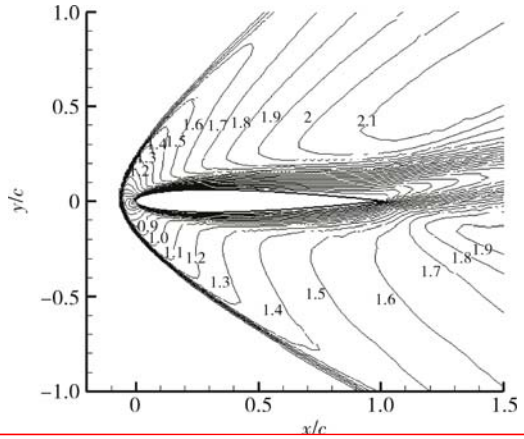

Fig. 14 Mach number contours of flow around the NACA0012 airfoil for case 2

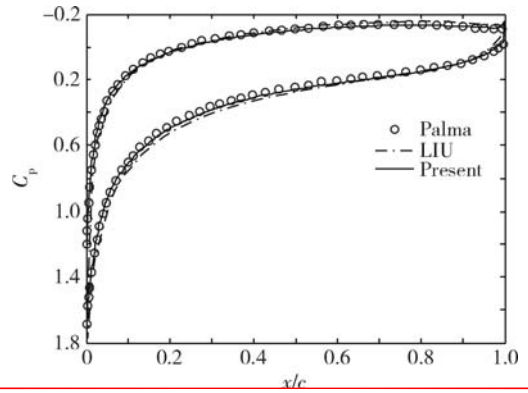

Fig. 15　Pressure coefficient distributions on the surface of the NACA0012 airfoil for case 2

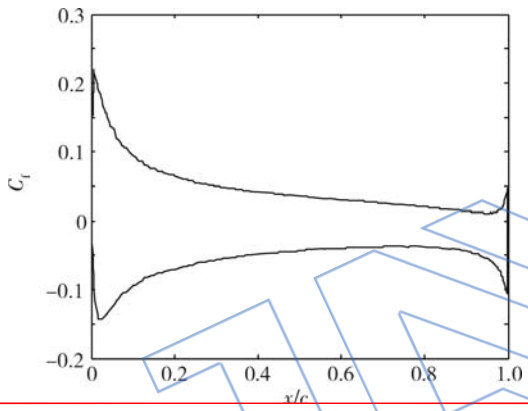

Fig. 16　Skin friction coefficient distributions on the surface of the NACA0012 airfoil for case 2

4　Conclusions

Cartesian grid is automatically generated after the geometry has been specified by users and adaptive refinements are operated according to the geometric information and solution of flow field. An altered CCST method has been proposed and validated on adaptively refined Cartesian grid. Current research covers incompressible/compressible subsonic, transonic and supersonic flow cases. Results obtained with this approach show good agreement with published structured grid/stretched Cartesian grid results, which indicate its efficiency in the simulations of viscous flows. Current research focus on the two-dimensional flow cases and this approach is applicable to three dimensional cases in principle while detailed complement needs to be further investigated.

References:

[1] Zeeuw D L D. A quadtree-based adaptively-refined Cartesian-grid algorithm for solution of the Euler equations[D]. Michigan: University of Michigan, 1993.

[2] Coirier W J. An adaptively-refined, Cartesian, cell-based scheme for the Euler and Navier-Stokes equations[D]. Michigan: University of Michigan, 1994.

[3] Colella P, Graves D T, Keen B J, et al. A Cartesian grid embedded boundary method for hyperbolic conservation laws[J]. Journal of Computational Physics, 2006, 211(1): 347-366.

[4] Udaykumar H S, Mittal R, Rampunggoon P, et al. A sharp interface Cartesian grid method for simulating flows with complex moving boundaries[J]. Journal of Computational Physics, 2001, 174(1): 345-380.

[5] Hua J, Lien F S, Yee E. Numerical simulation of detonation using an adaptive Cartesian cut-cell method combined with a cell-merging technique[J]. Computers & Fluids, 2010, 39(6): 1041-1057.

[6] Kirshman D J, Liu F. A gridless boundary condition method for the solution of the Euler equations on embedded Cartesian meshes with multigrid[J]. Journal of Computational Physics, 2004, 201(1): 119-147.

[7] Luo H, Baum J D, Lohner R. A hybrid Cartesian grid and gridless method for compressible flows[J]. Journal of Computational Physics, 2006, 214(2): 618-632.

[8] Liao W, Koh E P C, Tsai H M, et al. Euler calculations with embedded Cartesian grids and small-perturbation boundary conditions[J]. Journal of Computational Physics, 2010, 229(9): 3523-3542.

[9] Dadone A, Grossman B. Ghost-cell method for inviscid two-dimensional flows on Cartesian grids[J]. AIAA Journal, 2004, 42(12): 2499-2507.

[10] Dadone A. Towards a ghost-cell method for analysis of viscous flows on Cartesian-grids[R]. AIAA 2010-709, 2010.

[11] Tomasz P, Timur J L, Vincent G W. Adaptive mesh refinement-theory and applications[M]. New York: Springer, 2005.

[12] Liou M S. A sequel to AUSM: Part Ⅱ AUSM$^+$-up for all speeds[J]. Journal of Computational Physics, 2006, 214(1): 137-170.

[13] Wang Z J, Sun Y Z. Curvature-based wall boundary condition for the Euler equations on unstructured grids[J]. AIAA Journal, 2003, 41(1): 27-33.

[14] Ghia U, Ghia K N, Shin C T. High-*Re* solutions for incompressible flow using the Navier-Stokes equations and a

multigrid method[J]. Journal of Computational Physics, 1982,48(1):387-411.

[15] LIU Jianming. The immersed boundary method in compressible flows and its applications[D]. Nanjing: Nanjing University of Aeronautics and Astronautics,2010. (in Chinese)

[16] Bristeau M O,Glovinski R,Periaux J,et al. Numerical simulation of compressible Navier-Stokes flows[M]. Braunschweig: Vieweg,1987.

[17] Palma P D,Tullio M D D,Pascazio G,et al. An immersed-boundary method for compressible viscous flows[J]. Computers & Fluids,2006,35(7):693-702.